Chlorhexidine-Silver Nanoparticles Conjugation Leading to Antimicrobial Synergism but highly increased cytotoxicity

Nadezhda Ivanova *, Neli Ermenlieva, Lora Simeonova, Iliyan Kolev, Iliya Slavov, Velichka Andonova

Posted Date: 22 August 2023

doi: 10.20944/preprints202308.1493.v1

Keywords: silver nanoparticles; chlorhexidine; conjunction; complexation; surface functionalization; nano-scaled drug delivery; antimicrobial synergism; antiviral activity; Camellia sinensis catechins; green synthesis

Article

Chlorhexidine-Silver Nanoparticles Conjugation Leading to Antimicrobial Synergism but Highly Increased Cytotoxicity

Nadezhda Ivanova [1,*], Neli Ermenlieva [2], Lora Simeonova [3], Iliyan Kolev [4], Iliya Slavov [5] and Velichka Andonova [1]

[1] Department of Pharmaceutical Technologies, Faculty of Pharmacy, Medical University of Varna, 9000 Varna, Bulgaria; Nadejda.Ivanova@mu-varna.bg; Velichka.Andonova@mu-varna.bg
[2] Department of Microbiology and Virology, Faculty of Medicine, Medical University of Varna, 9000 Varna, Bulgaria.; Neli.Ermenlieva@mu-varna.bg
[3] Department of Virology, The Stephan Angeloff Institute of Microbiology, Bulgarian Academy of Sciences, 26 G. Bonchev Str., 1113 Sofia, Bulgaria; lora_simeonova@microbio.bas.bg
[4] Department of Pharmaceutical Chemistry, Faculty of Pharmacy, Medical University of Varna, 9000 Varna, Bulgaria; ilian.kolev@mu-varna.bg
[5] Department of Biology, Faculty of Pharmacy, Medical University of Varna, 9000 Varna, Bulgaria; ilia.slavov@mu-varna.bg
* Correspondence: Nadezhda.Ivanova@mu-varna.bg

Abstract: This study explored the potential synergism within chlorhexidine-silver nanoparticles conjugates against *Influenza type A*, *Staphylococcus aureus*, *Escherichia coli*, and *Candida albicans*. Silver nanoparticles (SN) were obtained by the reduction of silver ions with green tea total phenolic extract and conjugated with chlorhexidine (Cx). The particles were characterized by UV-Vis and FTIR spectroscopies, dynamic light scattering, X-ray diffraction, and transmission electron microscopy. A stable negatively-charged nano-silver colloid (ζ=-50.01) was obtained with an average hydrodynamic diameter of 92.34 nm. In the presence of chlorhexidine, the spectral data and the shift of the zeta potential to positive values (ζ=+44.59) revealed the successful sorption of the drug onto the silver surface. The conjugates (SN-Cx) demonstrated potentiation in the effects against *S. aureus* and *C. albicans*, and synergism against *E. coli* with minimal inhibitory concentrations of SN 5.5 μg/mL+Cx 8.8 μg/mL. The SN showed excellent, increasing with time, virucidal properties, and low toxicity. The coupling of the cationic chlorhexidine with nano-silver, however, did not reduce its intrinsic cytotoxicity on various cell lines (MDCK, BJ, and A549). The newly-synthesized antimicrobial agent presented with an extended and promising therapeutic spectrum and needs to be further evaluated on relevant to the designated route of administration three-dimensional cell models (e.g., nasal, bronchial, dermal, ocular, etc.).

Keywords: silver nanoparticles; chlorhexidine; conjunction; complexation; surface functionalization; nano-scaled drug delivery; antimicrobial synergism; antiviral activity; *Camellia sinensis* catechins; green synthesis

1. Introduction

In the last few years, several reports became available concerning the mutual or parallel utilization of silver nanoparticles (SN) and chlorhexidine (Cx) as a treatment/prophylactic strategy for specific infectious diseases. Both agents are widely studied and well-described in literature to possess distinct antimicrobial properties, which made a lot of scientists curious about a possible synergism, additive effects, or potentiation of their activities. Some interesting findings so far are of *Zhou et al.* who prepared a composite of poly(L-lactide) microcapsules of chlorhexidine with superficially adsorbed silver nanoparticles and found better antibacterial properties against *E. coli* and *S. aureus* with less usage of silver as compared to silver nanoparticles-carrying non-drug loaded microcapsules [1]; *Myronov et al.* reported that adding silver nanoparticles to chlorhexidine treatment improves infected wound healing through acceleration of bacteria elimination (*E. coli*, *P. aeruginosa*,

 doi:10.20944/preprints202308.1493.v1

S. aureus) and M2 macrophage polarization [2]; *Pernakov et al.* established accelerated would healing effect of silver nano-architectures and chlorhexidine, when combined, as compared with the single treatments with both agents, but did not observe any synergism in the antibacterial activity against *E. coli* and *P. aeruginosa* [3]. Other authors reported synergism or potentiation of SN and Cx against *Candida spp*. [4–6], *Enterococcus faecalis* [5,7], *Klebsiella pneumonia* [5], *Pseudomonas aeruginosa* [6,8], *Staphylococcus epidermidis* [6,8], and *Streptococcus mutans* [6,9]. To the best of our knowledge, yet cursorily addressed are the supramolecular interactions that may occur upon the addition of chlorhexidine to a nano-silver colloid and define the nature of the resultant effects. It would be speculative to seek any controversy or agreement in all the aforementioned findings since the surface functionality of nano-silver is indeed the crucial factor for any potential physicochemical and therapeutic properties of theirs and it is highly dependable on the preparation technique and the reducer used [10–13].

Today, due to pronounced antibacterial, antifungal, antiviral, and anticancer properties, SN are considered highly potent multifunctional units with a broad application range (e.g., in nanomedicine, dentistry, ecology, textile industry, cosmetics, etc.) [14–17]. The antimicrobial activity is primarily owed to the silver ions (Ag^+) released from the critically increased silver surface and subsequent oxidation or bonding to essential for the microorganisms' vitality, adhesion, and replication molecular factors [18–20]. Ever since the "green" synthetic methods were introduced, it has become a trend and a method of choice to obtain nano-silver colloids by reducing silver ions in dilute solutions of soluble silver salts with non-toxic reducers of natural origin — plant extracts, bacteria, yeast, fungi [11,21]. Being a rich source of primary and secondary metabolic products, most of them serve not only as reducers but also as capping (stabilizing) agents [11,22]. However, for the same reason, the various biological methods lead to highly differentiating functionality (shape, size, charge, redox potential, and superficial organic load — "cap") of the silver nanoparticles and this affects the efficiency of Ag^+ release; thus, depending on the reduction process and the surface properties, SN possess varying antimicrobial strength, toxicity, and not last —ability to be conjugated with other substrates [11,23].

Chlorhexidine (Cx) is a broad-spectrum local antiseptic with a biguanide structure and behavior of cationic surfactant in neutral and alkaline media. Slightly less pronounced are the antifungal properties of the compound in comparison with its antibacterial such [24,25]. Cx was considered a suitable substrate for conjugation to SN for several reasons: (1) when ionized, the molecule produces quaternary ammonium functional groups which can easily contribute to electrostatic adsorption of Cx on a negatively charged substrate [26,27] (such as the green-synthesized nano-silver in most cases [28,29]); (2) the presence of multiple basic N atoms sets a prerequisite for coordination with the silver nuclei [30], whereas the acidic NH are expected to step into a hydrogen bonding with the available phenolic groups in the organic cap [31–33]. It is yet unclear how these potential interactions may influence the therapeutic activity of SN and chlorhexidine itself, and whether they allow/determine potentiation or even synergistic action.

Our pilot study on "green" SN synthesis with green tea extracts confirmed better stability and purity of nano-silver colloids when catechin-rich phenolic extract is used for the reduction of silver ions rather than total green tea aqueous extract [34]. Furthermore, we obtained a clue for the synthesis' optimal parameters and the colloidal stability. In the present survey, we attempted to explore the production variables in more detail and establish the physicochemical nature of the resultant nano-silver colloids with a view to conjunction with chlorhexidine. We hypothesized that in a conjugated form, Cx and SN may present synergistic action against common pathogens, such as *Influenza virus*, *Staphylococcus aureus*, *Escherichia coli*, and *Candida albicans*.

2. Materials and Methods

2.1. Materials

2.1.1. Chemicals and reagents

 doi:10.20944/preprints202308.1493.v1

Sencha green tea was supplied by a local drugstore. Silver nitrate > 99.9% and sodium hydroxide pellets > 98% were purchased from Thermo Fisher Scientific, United Kingdom; Chlorhexidine diacetate salt hydrate ≥98%, Mw 625.55 g/mol was supplied from Sigma Aldrich, USA; all organic solvents were purchased from Sigma-Aldrich (USA) in analytical grade.

2.1.2. Bacteria and fungi

Escherichia coli ATCC 25922, *Staphylococcus aureus* ATCC 25923, and *Candida albicans* ATCC 10231 reference strains (MicroSwab) were obtained from Ridacom, Bulgaria. Brain-Hearth Infusion broth and Blood agar (HiMedia) were also purchased from Ridacom, Bulgaria.

2.1.3. Virus

Allantoic fluid and cell-derived seasonal *Influenza* virus laboratory strains A/Aichi/2/68 (H3N2) (D. I Ivanovsky Institute, Moscow, Russia) and A/Panama/07/99 (H3N2) (National Center for Infectious and Parasitic Diseases - NCIPD, Sofia, Bulgaria) were used at working doses of 100 $CCID_{50}$/mL (T=10–5,5 lg $CCID_{50}$/mL).

2.1.4. Cells

Madine-Darby canine kidney – MDCK (ATCC-CCL-34™) and human lung carcinoma A549 (ATCC-CCL-185™) epithelial cell lines, kindly provided by Dr. Cyril Barbesange, National Reference Center for *Influenza*, Sciensano, Belgium, as well as human diploid fibroblast cells BJ (ATCC-CRL-2522™), kindly provided by Dr. Kameliya Vinketova, Institute of Biology and Immunology of Reproduction "Acad. Kiril Bratanov" — Bulgarian Academy of Sciences (IBIR-BAS), were used. Cells were seeded at a density of $2.5x10^5$/mL at 37 °C in a 5% CO_2 incubator Thermo Forma 310 (Thermo Fisher Scientific, MA, USA), as a monolayer culture in 96-well plates (Corning® Costar®, USA) in growth medium DMEM (Gibco) or RPMI (Sigma) containing 5 and 10% fetal bovine serum (FBS) (Gibco), 3.7 mg/mL sodium bicarbonate, 10 μM HEPES buffer (AppliChem GmbH, Darmstadt, Germany), 100 U/mL Penicillin, 100 μg/mL Streptomycin, 25 μg/mL Amphotericin B for 24 h until monolayer confluence is reached.

2.2. Methods

2.2.1. Green tea total polyphenols extraction

A catechins-rich total phenolic fraction from Sencha green tea was isolated as reported previously [34]. Sencha green tea leaves were extracted with methanol, and the obtained filtrate was evaporated in a water bath. To the dried extract were added 10 mL of water and sodium chloride 10%. The mixture was placed in a separating funnel with 10 mL of ethyl acetate, and the combined ethyl acetate extracts were washed twice with water. After evaporation of the organic solvent, a mixture of catechins and other phenolic compounds was obtained.

2.2.2. Synthesis of silver nanoparticles (SN)

The reduction of silver ions was conducted with green tea phenolic fraction following the protocol established in our pilot study [34]. Briefly, silver nitrate ($AgNO_3$) solutions (1 mM and 2 mM) were obtained by dissolving the salt into distilled water under manual stirring at room temperature and proper dilution thereafter. The reductant, further referred to as C8, was prepared in the form of a green tea polyphenols aqueous solution with varying concentrations — 0.6–6.0 mg/mL, and alkalized to pH 8.0 with the aid of sodium hydroxide 10% solution (10–40 μl). The reaction vials were filled with 3.0 mL of silver nitrate solution and 0.5 mL of reductant were added. The mixtures were sealed and briefly shaken to homogenize. The vials were left to rest under dark conditions and ambient temperature overnight.

The silver nanosuspensions were purified from low-molecular weight unreacted phenolic compounds and ions through a dialysis procedure using Spectra/Por®2 Dialysis Membrane MWCO

 doi:10.20944/preprints202308.1493.v1

12–14 kDa (Spectrum Laboratories, Inc., USA). The membranes were prepared as recommended by the manufacturer. The sample was filled in a dialysis bag in a volume of 10.5 mL (the content of 3 reaction vials), immersed into 1000 mL dialysate (distilled water), and left under continuous stirring for 24 h. The process was allowed at room temperature and protected from the light environment. The resultant purified colloidal dispersion was evacuated from the dialysis bag with the help of a sterile syringe and a needle.

In order to preselect the most promising formulations overall, the samples were observed visually for colloidal stability (color, transparency, opalescence, turbidity, etc.) and spectrally – for confirmation of silver nanoparticles formation and their relative concentrations, for 7 days.

2.2.3. Determination of SN concentration

The concentration of SN [mg/mL] was determined after evaporation to dryness of 1.0 mL colloidal solution and following storage in a desiccator for at least 1 h. The change in mass of a glass petri used as a mediator for the purpose was recorded on an analytical balance. The experiment was performed in triplicate in a previously tempered room and with tempered samples at 25 °C.

2.2.4. Conjugation of SN and chlorhexidine

An optimized formulation of silver nanoparticles (SN) was subjected to conjugation with chlorhexidine (Cx). For this purpose, chlorhexidine acetate (Mw 625.55 g/mol) aqueous solution 3.75 mg/mL was prepared on a magnet stirrer (IKA® C-MAG HS 4, Germany) and added in varying volumes (0.5, 1.0, 1.5 mL) to a single reaction vial containing 3.5 mL of purified nano-silver suspension. The mixtures were sealed, briefly shaken to homogenize, and left to rest under dark conditions and ambient temperature. Whenever during the tests, a comparison needed to be done with the silver nanoparticles before conjunction, the latter were added equal volumes of distilled water (0.5, 1.0, or 1.5 mL, respectively), so that the nano-silver concentration in both conjugated and non-conjugated samples would be the same.

2.2.5. UV-Vis spectroscopy

UV-Vis scans of the samples were carried on a T60 UV-Vis spectrophotometer (PG Instruments, United Kingdom), in the spectral range from 220 to 800 nm; the spectral analysis was performed on day 2 after preparation (i.e., after dialysis completion), and on day 7 after preparation. Appropriate dilution (1:10 during the stage of SN optimization and 1:20 after conjunction with Cx) was carried out on all samples in advance. The total green tea phenolic extract and chlorhexidine acetate were also scanned for reference in the same spectral interval. UVWin 6.0 software was used for data curation and processing.

2.2.6. Dynamic light scattering/ Laser Doppler electrophoresis

The techniques of multi-angle dynamic light scattering (MADLS) and laser doppler electrophoresis (LDE) were applied for colloidal characterization of SN preselected samples and SN-Cx conjugated samples by average size (hydrodynamic diameter – d_H), size distribution, polydispersity, and zeta potential, respectively. Both studies were performed on Zetasizer Ultra red (λ=632.8 nm) (Malvern Panalytical Ltd., Malvern, UK) at 25 °C. Data was processed and obtained with the aid of ZS XPLORER software. The samples were scanned on day 2 after preparation and without any preliminary filtration.

2.2.7. Transmission electron microscopy (TEM)

TEM images were taken with a JEOL JEM 2100 (JEOL Ltd., Tokyo, Japan) transmission electron microscope at an accelerating voltage 200 kV.

2.2.8. FT-IR study

 doi:10.20944/preprints202308.1493.v1

The IR spectra were recorded on a Bruker Tensor II FTIR spectrometer in the 3750–400 cm^{-1} spectral region; accumulated by 32 scans with resolution of 4 cm^{-1}. A KBr tableting technique was used. The SN and SN-Cx samples were freeze-dried for the purpose without the addition of any stabilizers, e.g. cryoprotectants, lyoprotectants, etc.

2.2.9. X-ray Diffraction (XRD)

XRD analysis was carried out on SN and SN-Cx freeze-dried samples in a Panalytical Empyrean diffractometer (Malvern Panalytical Ltd., Malvern, UK). Chlorhexidine acetate crystalline powder was scanned for reference. The diffractograms were obtained by using a Cu-Kα source (λ = 1.5406 Å). The measurements were carried out at a 1 s/step scanning rate with a step size of 0.013°.

2.2.10. Antibacterial and antifungal activity

The antibacterial and antifungal activity of SN, Cx, and SN-Cx samples was tested against *Escherichia coli* ATCC 25922, *Staphylococcus aureus* ATCC 25923, and *Candida albicans* ATCC 10231 reference strains. The stock concentrations of the active agents were 0.7 mg/mL for SN samples, 1.13 mg/mL for Cx samples, and 0.7 mg/mL+1.13 mg/mL for SN-Cx samples, respectively. A serial two-fold dilution method was applied in eight test tubes in a row, containing 1.0 mL Brain Heart Infusion (BHI) broth. The resultant test concentrations were thus in the range of 1:2 to 1:256 dilution of the stock solutions. Next, 0.1 mL standardized to 0.5 McFarland turbidity equivalent microbial suspension was added to the vials. As positive controls were used samples of 1.0 mL BHI broth contaminated with 0.1 mL microbial suspension of each strain, whereas negative controls were set by mixing 1.0 mL BHI broth with each of the active agents. All tests were repeated in triplicate. The test vials containing *S. aureus* and *E. coli* were incubated for 24 h at 37 °C, and those with *C. albicans*—for 48 h at 35 °C. The minimal inhibitory concentration (MIC) of each substrate was determined thereafter as the lowest active concentration by which no visible turbidity is observed.

Minimal bactericidal/fungicidal concentrations (MBC/MFC) were determined by transferring all test suspensions with no visible turbidity in a single-bacterial-loop-volume onto blood agar. The so-obtained specimens were incubated once again under the same conditions as described above. The lowest concentration at which bacterial/fungal growth appeared to be inhibited 99.9% was reported as MBC/MFC.

2.2.11. Cytotoxicity (CC_{50}) and antiviral effect (IC_{50} and SI) evaluation by neutral red (NR) uptake assay

After infection of the cell monolayer and treatment with each of the active agents in a respective dilution of the stock solutions (starting from 1:10 and following a two-fold step), the 96-well plates (including virus and toxicity controls) were incubated in a thermostat at 37 °C and 5% CO_2 for 72 h. The treatment effect was first assessed visually under a microscope and then by staining with an NR dye [35]. The light absorbance of the samples was read at 540 nm on a microplate reader (Biotek Organon, West Chester, PA, USA).

The values obtained were used to calculate percent cell protection by applying the formula:

$$\% \text{ (CPE) inhibition} = [OD_{\text{test sample}} - OD_{\text{virus control}}]/[OD_{\text{toxicity control}} - OD_{\text{virus control}}]x100,$$

where CPE stands for cytopathic effect and OD—for optical density.

Toxicity was calculated as a percentage of untreated cell controls. The values obtained were used to calculate CC_{50}, IC_{50} и SI. The concentration of the substance causing 50% damage to cells after treatment is referred to as the 50% cytotoxic concentration or CC_{50}. The 50% inhibitory concentration (IC_{50}) is defined as the concentration of the substance that reduces viral replication by 50% compared to the untreated viral control. The selectivity index (SI) is represented by the CC_{50}/IC_{50} ratio.

2.2.12. Determination of the effect on extracellular virions - virucidal effect

Preprints (www.preprints.org) | NOT PEER-REVIEWED | Posted: 22 August 2023 doi:10.20944/preprints202308.1493.v1

Equivalent volumes of 100 $CCID_{50}$/mL virus suspension and the test samples (SN, Cx, or SN-Cx) were contacted in a 1:1 ratio and incubated at room temperature for different time intervals (5, 15, 30, and 60 min). The active agents were applied in their maximum tolerated concentrations (MTCs) or in two-fold and correspondingly ten-fold dilutions, as follows:

- SN 35 μg/mL (MTC) or 350 μg/mL (two-fold dilution of stock solution)
- Cx 2 μg/mL (MTC) or 113 μg/mL (10-fold dilution of stock solution)
- SN-Cx 1.2/2 μg/mL (MTC) or 70/113 μg/mL (10-fold dilution of stock solution)

The samples were then titrated by the end-point dilution method in a 24 h cell monolayer starting either directly from the contact sample (when applying MTC) or after an initial ten-fold dilution of the contact sample (incubated with two-fold or ten-fold diluted stock solution), with the content of residual infectious virus being assessed at 72 h post-infection by visual reading of the cytopathic effect under an inverted microscope and by NR uptake assay. Differences in CPE as Δlg between the treated groups and control virus suspension incubated for the same time intervals in the absence of the active agents were recorded.

2.2.13. Statistical data processing

The experiments were performed in two and three replicates for statistical reliability of the results. Data was processed using software Gen5®, Excel® Microsoft, Origin 8.5® и GraphPad Prism 6.0®.

3. Results and Discussion

3.1. Silver nanoparticles synthesis, optimization, and conjunction

All test formulations resulted in the formation of nano-silver, recognized by the immediate change in color to the yellow-reddish-brown scale and the surface plasmon resonance (SPR) peak manifesting in the range of 413–430 nm in all UV-Vis spectra. According to the spectral data (particularly, the absorption at the wavelength of the SPR extremum), the darkness of the color was found to correspond well with the concentration of the colloids. The highest nanosilver concentration with no visible signs of turbidity and/or sedimentation was established with sample 2C8R4.5, obtained in 2 mM silver nitrate solution with green tea polyphenols (C8) 4.5 mg/mL. Table 1 summarizes the information for all test compositions and the obtained UV-Vis spectral data; in Figure 1 the visual appearance of the samples within 7 days can be followed.

Table 1. Silver nanoparticles test formulations and UV-Vis spectral results.

Formulation Code	Silver nitrate conc., mM	Reductant (C8) conc., mg/mL *	Day 2		Day 7	
			λmax, nm	Abs	λmax, nm	Abs
1C8R0.6	1	0.6	426	0.306	430	0.480
2C8R0.6	2	0.6	425	0.436	429	0.570
1C8R1	1	1.0	423	0.617	429	0.742
2C8R1	2	1.0	425	0.774	428	0.887
1C8R1.5	1	1.5	425	0.755	429	0.911
2C8R1.5	2	1.5	425	0.948	430	1.122
1C8R3	1	3	417	1.346	418	1.391
2C8R3	2	3	421	1.825	424	1.902
1C8R4.5	1	4.5	416	1.382	415	1.369
2C8R4.5	**2**	**4.5**	**421**	**2.372**	**422**	**2.385**

Preprints (www.preprints.org) | NOT PEER-REVIEWED | Posted: 22 August 2023 doi:10.20944/preprints202308.1493.v1

1C8R6	1	6	413	1.444	415	1.496
2C8R6 **	2	6	417	2.587	420	2.758

* The reductant volume was kept constant at 0.5 mL; ** Turbidity and a slight sediment was formed in a few days of storage.

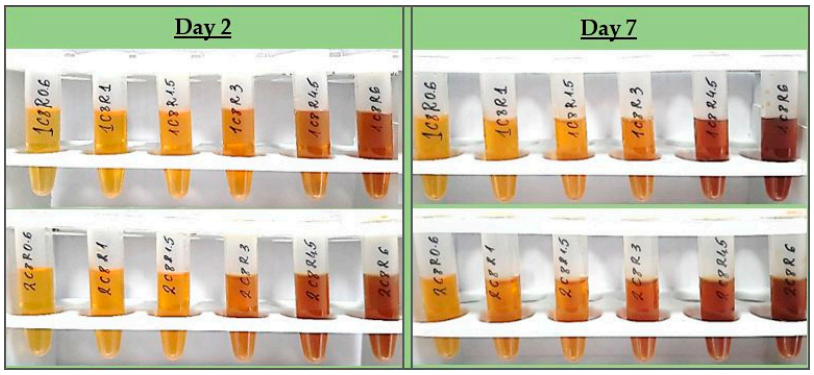

Figure 1. Visual appearance of SN samples on day 2 after preparation (right after dialysis) and on day 7 after preparation.

The colloidal stability of samples 2C8R[1.5–4.5] was confirmed by zeta potential analysis. With the zeta potential of sample 2C8R4.5 being the highest among all by absolute value — [-50.01 mV], the initial observation was confirmed for it to be the composition of choice for further analyses and conjunction with Cx. Through evaporation to dryness, the nano-silver content (including the organic load) in the sample in question was established to be 1.005±0.012 mg/mL.

As expected upon successful sorption of chlorhexidine diacetate (Cx) onto the silver nanoparticles surface, the colloids acquired a positive zeta potential; favorably for the purpose of the study, the latter was found to reach maximal absolute values by samples obtained with the highest investigated drug load, i.e., 1.5 mL of Cx 3.75 mg/mL solution. At such dilution of the colloid, the nano-silver concentration drops to 0.7 mg/mL. Table 2 summarizes the data from the zeta potential measurements.

Table 2. Zeta potential of SN and SN-Cx samples.

Formulation code	Cx 3.75 mg/mL vol. (mL)	Cx final conc. in solution, mg/mL	Zeta potential, mV
2C8R1.5	n/a	n/a	-43.45
2C8R3	n/a	n/a	-39.06
2C8R4.5	**n/a**	**n/a**	**-50.01**
2C8R1.5 Cx+	0.5	0.47	+31.24
2C8R1.5 Cx++	1.0	0.83	+33.74
2C8R1.5 Cx+++	1.5	1.13	+36.2
2C8R3 Cx+	0.5	0.47	+40.02
2C8R3 Cx++	1.0	0.83	+44.34
2C8R3 Cx+++	1.5	1.13	+42.44
2C8R4.5 Cx+	0.5	0.47	+41.22
2C8R4.5 Cx++	1.0	0.83	+43.78
2C8R4.5 Cx+++	**1.5**	**1.13**	**+44.59**

Preprints (www.preprints.org) | NOT PEER-REVIEWED | Posted: 22 August 2023 doi:10.20944/preprints202308.1493.v1

The electron microscopy and the dynamic light scattering results confirmed significant enlargement in the conjugated particles' diameter and hydrodynamic diameter (d_H) as compared to the SN alone. These observations are in accordance with the shift in the SPR peak of the conjugates to higher values (SN λ_{max}=421 nm < SN-Cx λ_{max}=439 nm). Macroscopically, the conjugated nanosuspension retained in general the visual appearance of the unconjugated sample but presented with slightly more pronounced opalescence. Negligible sediment was repeatedly observed after a few days of storage but was easily resuspended upon shaking. Figures 2A and 2B show the UV spectra, TEM micrographs, the zeta potential distribution and size analysis by hydrodynamic diameter of SN sample 2C8R4.5 and the optimal SN-Cx conjugated form, namely 2C8R4.5Cx+++.

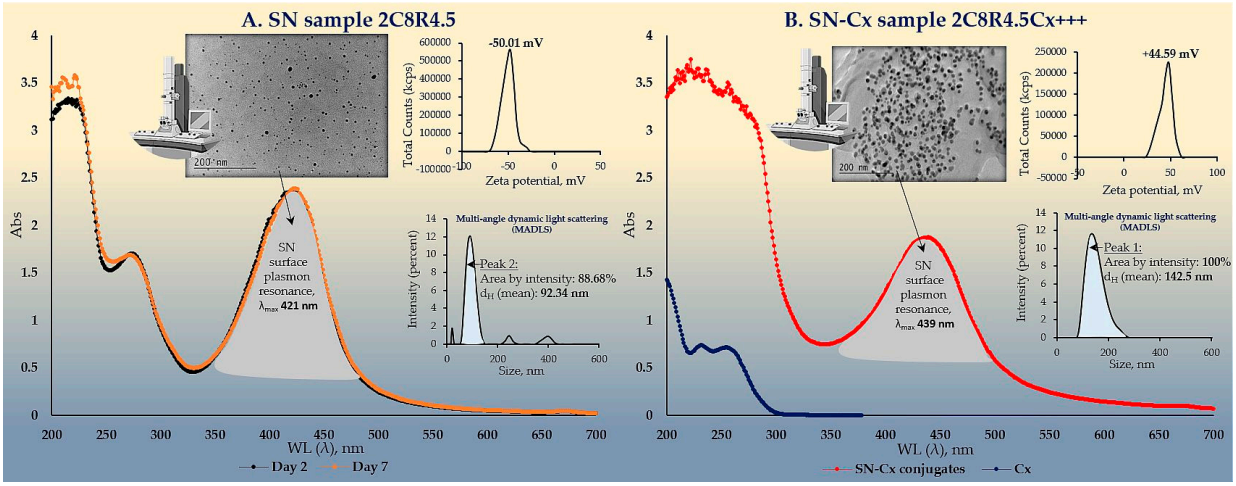

Figure 2. UV-Vis spectra, TEM micrographs, zeta potential distribution, and size analysis by MADLS of A. SN sample 2C8R4.5 and B. SN-Cx sample 2C8R4.5Cx+++.

3.2. FTIR spectroscopy

In the infrared spectrum of the phenolic extract (Figure 3), the presence of multiple bands of relatively high intensity, characteristic of the four catechin diastereoisomers, was observed at 1627, 1625, 1612, 1520, 1240, 1202, 1145, 1096, and 1037 cm^{-1} [36]. Bands falling in the range of 1400 to 1650 cm^{-1} are considered to be characteristic of the catechin's aromatic (benzenoid) residues [37]. In the same spectrum, the remaining high-intensity bands (with maxima at 1037, 1145, 1240, and 1285 cm^{-1}) are associated with the inherent to phenolic and alcohol groups C—O stretching and δ(O—H) vibrations, and those registered at the higher wavelengths (at 766 and 823 cm^{-1}) - with the out-of-plane C_{ar}—H modes.

Preprints (www.preprints.org) | NOT PEER-REVIEWED | Posted: 22 August 2023 doi:10.20944/preprints202308.1493.v1

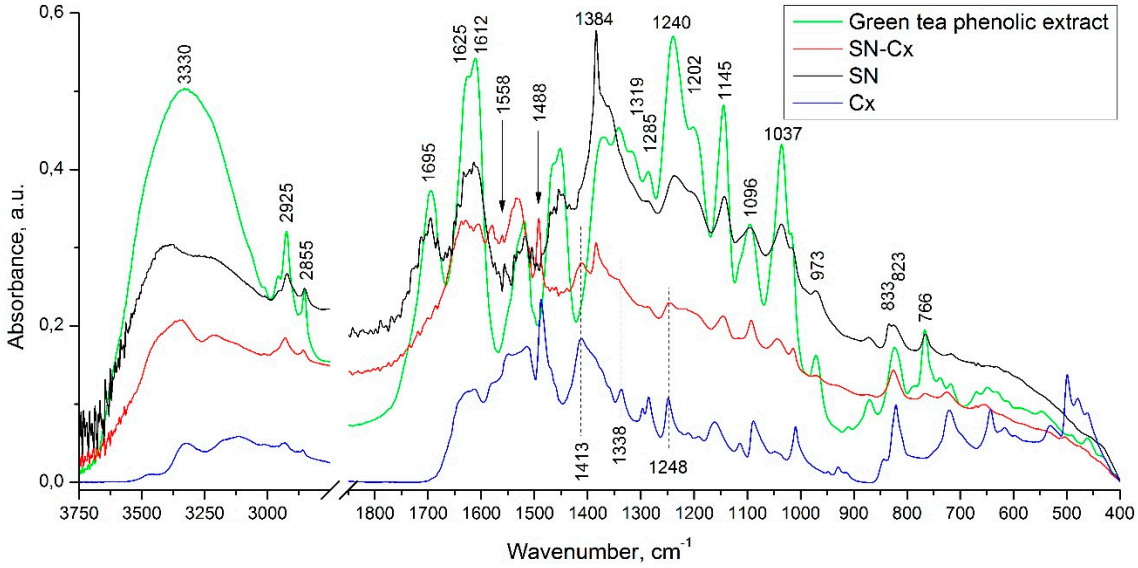

Figure 3. FTIR spectra of Green tea phenolic extract (green line), SN (black line), Cx (blue line), and SN-Cx (red line) samples.

In the spectrum of the SN sample, the presence of all the above-mentioned absorption bands, characteristic of the phenolic extract used, was observed. As the reason for the preserved IR catechin imprint in the spectrum of the SN sample, we would present the tendency of catechins to sorb on the surface of the formed with their participation metal nanoparticles [29]. It should be noted that in the spectrum of the sample in question, the appearance of bands characteristic of the asymmetric and symmetric stretching vibrations of NO_2 groups (at 1558 and 1384 cm^{-1}) is also registered. As an additional, but debatable indication of the presence of the latter, we would point to the presence of the low-intensity band at 833 cm^{-1} - band characteristic of $C_{ar}—NO_2$ oscillations. The reason for the presence of this functional group will not be discussed here, but it is assumed that in the course of the imposed redox process, nitration of the organic substrate also takes place.

Moreover, comparing the spectra of the Cx and SN-Cx samples, the presence of the used anti-infective drug in the composition of the target nanoparticles was established.

3.3. X-Ray diffraction (XRD)

The X-Ray diffractograms of silver nanoparticles (SN), their conjugates with chlorhexidine (SN-Cx), and chlorhexidine acetate (Cx) are shown in Figure 4. Recognizable in the conjugated and non-conjugated nanoparticles' spectra is the standard diffraction pattern of elemental silver (Ag) of face-centered cubic symmetry. The latter is distinguished by reflections at 2θ 38°, 44°, 64°, and 77°, corresponding to the (111), (200), (220), and (311) planes [38–41]. The broad scattering and the lack of sharp, intense peaks in the SN and SN-Cx spectra reveal the substantial presence of amorphous matter and small crystallite size [38,40]. None of the intrinsic chlorhexidine diffraction peaks (e.g., 2θ 19.8°, 20.4°, 25.1°) [42–44] was evident by the conjugated nano-silver form; this observation confirms the amorphization of the drug upon loading onto the metal delivery platforms. The presence of crystalline silver oxide — Ag_2O, standardly recognized by intense reflections at 28° and 32° of the (110) and (111) planes [45–47] was not detected in the nano samples. However, an extra peak was recorded in the X-ray spectrum of SN at 29°, which might be a result of catechin crystalline segments in the sample [48] that get spectrally disguised or amorphized in the presence of chlorhexidine.

Preprints (www.preprints.org) | NOT PEER-REVIEWED | Posted: 22 August 2023 doi:10.20944/preprints202308.1493.v1

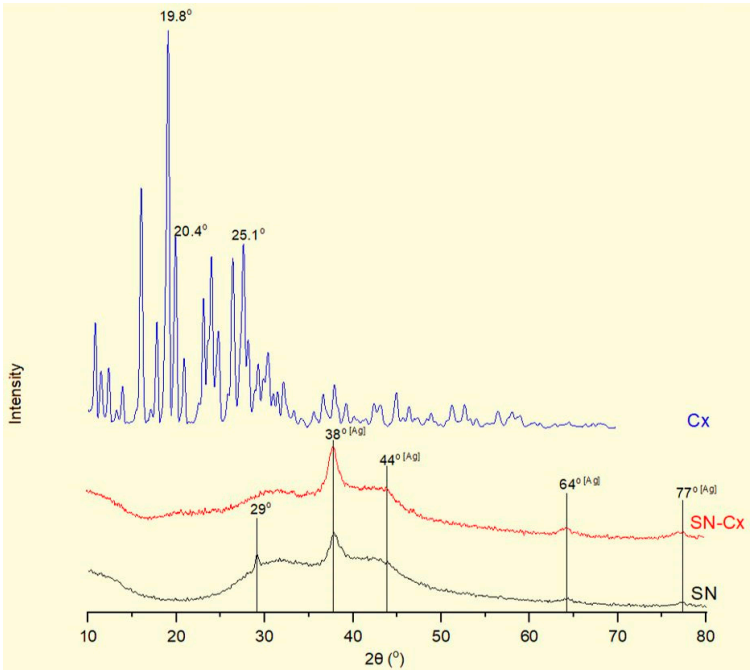

Figure 4. XRD of SN sample 2C8R4.5 (black line), SN-Cx sample 2C8R4.5Cx+++ (red line), and chlorhexidine diacetate (blue line).

3.4. Antibacterial and antifungal activity

3.4.1. Minimal inhibitory concertation (MIC)

Inhibitory activity of SN alone against E. coli was recorded at relatively high concentrations — 175 μg/mL (e.g., dilution 1:4); antimicrobial activity against the other two pathogens — S. aureus and C. albicans did not manifest at the investigated concentrations. It is worth mentioning that a slight opalescence was observed even within the negative controls with SN, which directed our attention rather to the MBC/MFC results. Such opalescence is likely a result of a colloidal instability of the SN samples in the electrolytes-rich fluid growth medium.

When Cx was tested alone, MICs of 35.3 μg/mL (dilution 1:32) against E. coli and 17.7 μg/mL (dilution 1:64) against S. aureus and C. albicans were established. The SN-Cx conjugates exceeded these results by demonstrating MIC against all strains at SN 5.5 μg/mL+Cx 8.8 μg/mL (dilution 1:128). Only vials from the last in-row tested concentrations, corresponding to 1:256 dilutions, remained turbid. The negative controls here were clear and transparent.

3.4.2. Minimal bactericidal/fungicidal concentration (MBC/MFC)

The MBC/MFC study confirmed the lack of antimicrobial activity of SN alone against S. aureus and C. albicans, whereas the established MIC against E. coli — 175 μg/mL, was shown to correspond to the MBC as well. The results from the MBC/MFC tests of Cx and SN-Cx conjugates are presented in Figure 5 and summarized in Table 3.

Preprints (www.preprints.org) | NOT PEER-REVIEWED | Posted: 22 August 2023 doi:10.20944/preprints202308.1493.v1

Figure 5. Seeds of Cx and SN-Cx diluted suspensions on Blood agar.

Table 3. Zeta potential of SN and SN-Cx samples.

Infectious strain	MBC/MFC		
	SN (µg/mL)	Cx (µg/mL)	SN+Cx (µg/mL)
E. coli	175	141.3	SN 5.5 + Cx 8.8
S. aureus	not established	35.3	SN 10.9 + Cx 17.7
C. albicans	not established	not established	SN 10.9 + Cx 17.7

According to these results, the conjugates (SN-Cx) demonstrate potentiation in the effects of the single components against S. aureus and C. albicans, and synergism against E. coli. Additionally, the observation of some authors was confirmed that Gram-negative microorganisms are in general more susceptible to the presence of silver nanoparticles than Gram-positive bacteria, likely due to the thicker cellular wall-peptidoglycan layer of the latter and the thus restricted penetration of Ag^+ [49,50].

3.4. Cytotoxicity, antiviral, and virucidal activity

The results for CC_{50}, IC_{50}, SI, and virucidal activity (Δlg) of the SN, Cx, and SN-Cx samples are presented in the following Tables 4–6.

Table 4. Cytotoxicity in MDCK, A549, and BJ cells and antiviral activity in an experimental infection with 100 $CCID_{50}$/mL *influenza* virus A/Aichi/2/68 (H3N2) in MDCK line.

Active agent	Cell line	Cytotoxicity	Antiviral effect	
		CC_{50} (µg/mL) ±SD	IC_{50} (µg/mL)	SI
SN	MDCK	56.4 ± 0.4	43.6 ± 16.6	1.29
Cx	MDCK	2.5 ± 0.7	-	-
SN-Cx	MDCK	1.6/2.6 ± 0.1	-	-
SN	A549	60.7 ± 0.3	n.d.	n.d.
Cx	A549	5.3 ± 0.7	n.d.	n.d.
SN-Cx	A549	3.6/5.8 ± 0.2	n.d.	n.d.

Preprints (www.preprints.org) | NOT PEER-REVIEWED | Posted: 22 August 2023 doi:10.20944/preprints202308.1493.v1

SN	BJ	16.9 ± 0.4	n.d.	n.d.
Cx	BJ	2.2 ± 0.1	n.d.	n.d.
SN-Cx	BJ	1.5/2.4 ± 0.5	n.d.	n.d.

SD — standard deviation; n.d. — not done.

Table 5. Virucidal activity of maximal tolerated concentrations (MTC) of SN, Cx, and SN-Cx against 100 $CCID_{50}$/mL *Influenza* virus A/Aichi/2/68 (H3N2) and titration from the contact sample in MDCK cells.

Active agent	**Δlg**			
	5 min	15 min	30 min	60 min
SN 35 μg/mL	2.5	2.66	3.00	3.00
Cx 2.0 μg/mL	0	0	0	0
SN-Cx 1.2/2.0 μg/mL	0	0	0.33	0.33

Table 6. Virucidal activity of SN 350 μg/mL, Cx 113 μg/mL, and SN-Cx 70.0/113.0 μg/mL against 100 $CCID_{50}$/mL *Influenza* virus A/Panama/2007/99 (H3N2) and titration from a 10-fold dilution of the contact sample in MDCK cells.

Active agent	**Δlg**			
	5 min	15 min	30 min	60 min
SN 350 μg/mL	2	2.33	2.5	3
Cx 113 μg/mL	1	1.33	1.66	1.66
SN-Cx 70.0/113.0 μg/mL	1	1.33	1.66	2

The determined CC_{50} values of SN in MDCK, A549, and BJ cell cultures — viz., 56.4, 60.7, and 16.9 μg/mL, respectively, reveal SN as an active agent with relatively low to moderate toxicity. In MDCK cells, the CC_{50} of Cx alone was 2.6 and 2.5 μg/mL in the conjugated form of SN-Cx. In A549 cell cultures, the same respective values were 5.3 and 5.8 μg/mL; in human BJ fibroblasts —2.2 and 2.4 μg/mL. According to these results, Cx and the Cx-bearing conjugated form (SN-Cx) could be defined as agents with high toxicity. SN showed a weak effect on the replication of the A/Aichi/2/68 virus with a mean IC_{50}=43.6 μg/mL and SI=1.29. In the applied concentrations, the Cx and SN-Cx samples did not affect the replication of Influenza virus A/Aichi/2/68 (H3N2) in MDCK cell cultures in a dose-response experimental design.

A strong virucidal effect was established at the SN MTC of 35 μg/mL from 5 to 60 min. The absence of virucidal effect of Cx and SN-Cx against the investigated Influenza strain A/Aichi/2/68 (H3N2) is probably due to the low working concentrations of 2 μg/mL for Cx and 1.2/2 μg/mL for SN-Cx, respectively, applied because of the substrates' high toxicity.

The distinguished time-dependent virucidal effect of SN was confirmed against Influenza strain A/Panama/2007/99 (H3N2) as well, at the working concentration of 350 μg/mL upon contact and following 10-fold dilution prior to titration in the cell monolayer. The virucidal activity of Cx and SN-Cx against Influenza A/Panama/2007/99 (H3N2) virus was assessed as weak (5 and 15 min) to moderate (30 and 60 min) when higher concentrations (than in the former experiment against A/Aichi/2/68 (H3N2) strain) were in contact with the virus—namely, Cx 113.0 μg/mL and SN-Cx 70.0/113.0 μg/mL, respectively. Before titration in the cell monolayer, additional ten-fold dilutions were still performed so that non-toxic concentrations are applied. However, residual toxicity of the

Cx and SN-Cx preparations in the greater dilutions and respective interference with the CPE could explain the established lower virucidal activity as compared to the SN alone.

4. Conclusions

Chlorhexidine diacetate was successfully adsorbed onto the "green"-synthesized silver nanoparticles' negatively-charged surface. The so-obtained colloidal solution retained satisfactory physical stability for the time being of the survey. The resultant conjugates presented with enhanced antimicrobial activity judging by the results on common pathogens such as *Escherichia coli*, *Staphylococcus aureus*, and *Candida albicans*. The addition of nano-silver to chlorhexidine solution decreased significantly the minimal bactericidal/fungicidal concentrations for all tested bacteria and fungi. Moreover, at the investigated concentrations, a fungicidal activity of chlorhexidine alone against *C. albicans* was not established, whereas the unconjugated silver nanoparticles did not show to inhibit or kill *S. aureus* and *C. albicans* independently. As expected, the cationic surfactant chlorhexidine exhibited high toxicity on Madine-Darby canine kidney line, human fibroblasts, and lung carcinoma cells; this was so regardless of the much lower active concentrations applied (0.00004–0.11%) in comparison to the standard such in commercial local antiseptic products (0.02–0.2%). The effect did not attenuate upon the conjugation of the drug to nano-silver vehicles which limited the active concentration range to be tested for antiviral and virucidal activity on *Influenza* type A. The unconjugated silver nanoparticles, on the other side, demonstrated good tolerability and low toxicity. Therefore, a relatively high concentration of 35 μg/ml was applied and showed a weak antiviral effect but distinct virucidal properties. Regardless of the latter ascertainments, the chlorhexidine-silver nanoparticles conjugate expressed a pronounced synergistic action and an extended spectrum of antimicrobial activity. It is relevant to seek the applicability and efficacy of this promising newly-synthesized agent in pharmaceutical dosage forms for dermal, nasal, oromucosal, ocular administration, or else. This prospect will require more specific and bio-relevant tolerability tests on 3D and organoid cultures.

Author Contributions: Conceptualization, N.I.; methodology, N.I, N.E., L.S., I.K., and I.S..; software, N.I, L.S., and I.K.; validation, I.K. and V.A..; formal analysis, N.I, N.E., L.S., and I.K.; investigation, N.I, N.E., L.S., and I.K.; resources, N.I, N.E., L.S., I.K., I.S., and V.A.; data curation, N.I, N.E., L.S., and I.K.; writing—original draft preparation, N.I, N.E., L.S., and I.K.; writing—review and editing, V.A.; visualization, N.I.; supervision, V.A.; project administration, N.I. and V.A.; funding acquisition, N.I. All authors have read and agreed to the published version of the manuscript.

Funding: This work was funded by Fund "Nauka" at the Medical University of Varna, Bulgaria, grant number Project No. 20016.

Institutional Review Board Statement: Not applicable.

Informed Consent Statement: Not applicable.

Data Availability Statement: Not applicable.

Conflicts of Interest: The authors declare no conflict of interest.

References

1. Zhou, Y.; Hu, K.; Guo, Z.; Fang, K.; Wang, X.; Yang, F.; Gu, N. PLLA microcapsules combined with silver nanoparticles and chlorhexidine acetate showing improved antibacterial effect. *Materials Science and Engineering: C* **2017**, *78*, 349–353. https://doi.org/10.1016/j.msec.2017.04.100
2. Myronov, P.; Sulaieva, O.; Korniienko, V.; Banasiuk, R.; Vielikov, M.; Husak, Ye.; Pernakov, M.; Deineka, V.; Yusupova, A.; Hristova, M.-T.; Savchenko, A.; Holubnycha, V.; Pogorielov, M. Combination of Chlorhexidine and Silver Nanoparticles: an Efficient Wound Infection and Healing Control System. *BioNanoScience* **2021,** *11(2)*, 256–268. https://doi.org/10.1007/s12668-021-00834-5
3. Pernakov, M.; Ermini, M. L.; Sulaieva, O.; Cassano, D.; Santucci, M.; Husak, Y.; Korniienko, V.; Giannone, G.; Yusupova, A.; Liubchak, I.; Hristova, M. T.; Savchenko, A.; Holubnycha, V.; Voliani, V.; Pogorielov, M. Complementary Effect of Non-Persistent Silver Nano-Architectures and Chlorhexidine on Infected Wound Healing. *Biomedicines* **2021**, *9(9)*, 1215. https://doi.org/10.3390/biomedicines9091215

4. Monteiro, D. R.; Silva, S.; Negri, M.; Gorup, L. F.; de Camargo, E. R.; Oliveira, R.; Barbosa, D. B.; Henriques, M. Antifungal activity of silver nanoparticles in combination with nystatin and chlorhexidine digluconate against Candida albicans and Candida glabrata biofilms. *Mycoses* **2013**, *56(6)*, 672–680. https://doi.org/10.1111/myc.12093
5. Charannya, S.; Duraivel, D.; Padminee, K.; Poorni, S.; Nishanthine, C.; Srinivasan, M. Comparative evaluation of antimicrobial efficacy of silver nanoparticles and 2% chlorhexidine gluconate when used alone and in combination assessed using agar diffusion method: An In vitro study. *Contemporary Clinical Dentistry*, **2018**, *9(6)*, 204. https://doi.org/10.4103/ccd.ccd_869_17
6. Steckiewicz, K. P.; Cieciórski, P.; Barcińska, E.; Jaśkiewicz, M.; Narajczyk, M.; Bauer, M.; Kamysz, W.; Megiel, E.; Inkielewicz-Stepniak, I. Silver Nanoparticles as Chlorhexidine and Metronidazole Drug Delivery Platforms: Their Potential Use in Treating Periodontitis. *International Journal of Nanomedicine* 2022, *17*, 495–517. https://doi.org/10.2147/ijn.s339046
7. Gholami, A.; Ghezelbash, K.; Asheghi, B.; Abbaszadegan, A.; Amini, A. An In Vitro Study on the Antibacterial Effects of Chlorhexidine-Loaded Positively Charged Silver Nanoparticles on Enterococcus faecalis. *Journal of Nanomaterials* **2022**, *2022*, 1–8. https://doi.org/10.1155/2022/6405772
8. Ben-Knaz, R.; Pedahzur, R.; Avnir, D. Bioactive doped metals: high synergism in the bactericidal activity of chlorhexidine@silver towards wound pathogenic bacteria. *RSC Advances* **2013**, *3(21)*, 8009. https://doi.org/10.1039/c3ra41196f
9. Lu, M.; Ge, Y.; Qiu, J.; Shao, D.; Zhang, Y.; Bai, J.; Zheng, X.; Chang, Z.; Wang, Z.; Dong, W.; Tang, C. Redox/pH dual-controlled release of chlorhexidine and silver ions from biodegradable mesoporous silica nanoparticles against oral biofilms. *International Journal of Nanomedicine* **2018**, *13*, 7697–7709. https://doi.org/10.2147/ijn.s181168
10. Ahmad, F.; Salem-Bekhit, M. M.; Khan, F.; Alshehri, S.; Khan, A.; Ghoneim, M. M.; Wu, H.-F.; Taha, E. I.; Elbagory, I. Unique Properties of Surface-Functionalized Nanoparticles for Bio-Application: Functionalization Mechanisms and Importance in Application. *Nanomaterials* **2022**, *12(8)*, 1333. https://doi.org/10.3390/nano12081333
11. Ivanova, N.; Gugleva, V.; Dobreva, M.; Pehlivanov, I.; Stefanov, S.; Andonova, V. Silver Nanoparticles as Multi-Functional Drug Delivery Systems. In *Nanomedicines*. Farrukh, M. A. Ed.; IntechOpen; London, UK, 2018; pp. 71–91. https://doi.org/10.5772/intechopen.80238
12. Zhang, X.-F.; Liu, Z.-G.; Shen, W.; Gurunathan, S. Silver Nanoparticles: Synthesis, Characterization, Properties, Applications, and Therapeutic Approaches. *International Journal of Molecular Sciences* **2016**, *17(9)*, 1534. https://doi.org/10.3390/ijms17091534
13. Wu, F.; Harper, B. J.; Harper, S. L. Differential dissolution and toxicity of surface functionalized silver nanoparticles in small-scale microcosms: impacts of community complexity. *Environmental Science: Nano* **2017**, *4(2)*, 359–372. https://doi.org/10.1039/c6en00324a
14. Noah, N. Green synthesis: Characterization and application of silver and gold nanoparticles. In *Green Synthesis, Characterization and Applications of Nanoparticles*. Shukla, A. K.; Iravani, S. Eds.; Elsevier Inc., Netherlands, 2019; pp. 111–135. https://doi.org/10.1016/b978-0-08-102579-6.00006-x
15. Ong, W. T. J.; Nyam, K. L. Evaluation of silver nanoparticles in cosmeceutical and potential biosafety complications. *Saudi Journal of Biological Sciences* **2022**, *29(4)*, 2085–2094. https://doi.org/10.1016/j.sjbs.2022.01.035
16. Mallineni, S. K.; Sakhamuri, S.; Kotha, S. L.; AlAsmari, A. R. G. M.; AlJefri, G. H.; Almotawah, F. N.; Mallineni, S.; Sajja, R. Silver Nanoparticles in Dental Applications: A Descriptive Review. *Bioengineering* **2023**, *10(3)*, 327. https://doi.org/10.3390/bioengineering10030327
17. Huang, C.; Cai, Y.; Chen, X.; Ke, Y. Silver-based nanocomposite for fabricating high performance value-added cotton. *Cellulose* **2021**, *29(2)*, 723–750. https://doi.org/10.1007/s10570-021-04257-z
18. Anees Ahmad, S.; Sachi Das, S.; Khatoon, A.; Tahir Ansari, M.; Afzal, Mohd.; Saquib Hasnain, M.; Kumar Nayak, A. Bactericidal activity of silver nanoparticles: A mechanistic review. *Materials Science for Energy Technologies* **2020**, *3*, 756–769. https://doi.org/10.1016/j.mset.2020.09.002
19. Yin, I. X.; Zhang, J.; Zhao, I. S.; Mei, M. L.; Li, Q.; Chu, C. H. The Antibacterial Mechanism of Silver Nanoparticles and Its Application in Dentistry. *International Journal of Nanomedicine* **2020**, *15*, 2555–2562. https://doi.org/10.2147/ijn.s246764
20. Bruna, T.; Maldonado-Bravo, F.; Jara, P.; Caro, N. Silver Nanoparticles and Their Antibacterial Applications. *International Journal of Molecular Sciences* **2021**, *22(13)*, 7202. https://doi.org/10.3390/ijms22137202
21. Vishwanath, R.; Negi, B. Conventional and green methods of synthesis of silver nanoparticles and their antimicrobial properties. *Current Research in Green and Sustainable Chemistry* **2021**, *4*, 100205. https://doi.org/10.1016/j.crgsc.2021.100205
22. Guilger-Casagrande, M.; Lima, R. de. Synthesis of Silver Nanoparticles Mediated by Fungi: A Review. *Frontiers in Bioengineering and Biotechnology* **2019**, *7*. https://doi.org/10.3389/fbioe.2019.00287

23. Prasher, P.; Sharma, M. *SILVER NANOPARTICLES: Synthesis, Functionalization and Applications*; Bentham Science Publishers, UAE; pp. 65–85. https://doi.org/10.2174/9789815050530122010006
24. John, V.; Weddell, J. A.; Shin, D. E.; Jones, J. E. Gingivitis and Periodontal Disease. In *McDonald and Avery's Dentistry for the Child and Adolescent*; Dean, J. A. Ed.; Elsevier Inc., Netherlands, 2016; pp. 243–273. https://doi.org/10.1016/b978-0-323-28745-6.00014-4
25. Mueller, R. S. Topical dermatological therapy. In *Small Animal Clinical Pharmacology*; Maddison, J. E., Page, S. W., Church, D. B. Eds.; Elsevier Inc., Netherlands, 2008; pp.546–556. https://doi.org/10.1016/b978-070202858-8.50026-9
26. Jou, S. K.; Malek, N. A. N. N. Characterization and antibacterial activity of chlorhexidine loaded silver-kaolinite. *Applied Clay Science* **2016**, *127–128*, 1–9. https://doi.org/10.1016/j.clay.2016.04.001
27. Cole, M.; Hobden, J.; Warner, I. Recycling Antibiotics into GUMBOS: A New Combination Strategy to Combat Multi-Drug-Resistant Bacteria. *Molecules* **2015**, *20(4)*, 6466–6487. https://doi.org/10.3390/molecules20046466
28. Riaz, M.; Mutreja, V.; Sareen, S.; Ahmad, B.; Faheem, M.; Zahid, N.; Jabbour, G.; Park, J. Exceptional antibacterial and cytotoxic potency of monodisperse greener AgNPs prepared under optimized pH and temperature. *Scientific Reports* **2021,** *11(1)*. https://doi.org/10.1038/s41598-021-82555-z
29. Meesaragandla, B.; Hayet, S.; Fine, T.; Janke, U.; Chai, L.; Delcea, M. Inhibitory Effect of Epigallocatechin Gallate-Silver Nanoparticles and Their Lysozyme Bioconjugates on Biofilm Formation and Cytotoxicity. *ACS Applied Bio Materials* **2022**, *5(9)*, 4213–4221. https://doi.org/10.1021/acsabm.2c00409
30. Liang, X.; Luan, S.; Yin, Z.; He, M.; He, C.; Yin, L.; Zou, Y.; Yuan, Z.; Li, L.; Song, X.; Lv, C.; Zhang, W. Recent advances in the medical use of silver complex. *European Journal of Medicinal Chemistry* **2018**, *157*, 62–80. https://doi.org/10.1016/j.ejmech.2018.07.057
31. B. Aziz, S.; Hussein, G.; Brza, M. A.; J. Mohammed, S.; T. Abdulwahid, R.; Raza Saeed, S.; Hassanzadeh, A. Fabrication of Interconnected Plasmonic Spherical Silver Nanoparticles with Enhanced Localized Surface Plasmon Resonance (LSPR) Peaks Using Quince Leaf Extract Solution. *Nanomaterials* 2019, *9(11),* 1557. https://doi.org/10.3390/nano9111557
32. Nemčeková, K.; Svitková, V.; Sochr, J.; Gemeiner, P.; Labuda, J. Gallic acid-coated silver nanoparticles as perspective drug nanocarriers: bioanalytical study. *Analytical and Bioanalytical Chemistry* **2022**, *414(18)*, 5493–5505. https://doi.org/10.1007/s00216-022-03955-2
33. Rezazadeh, N. H.; Buazar, F.; Matroodi, S. Synergistic effects of combinatorial chitosan and polyphenol biomolecules on enhanced antibacterial activity of biofunctionalized silver nanoparticles. *Scientific Reports* **2020**, *10(1)*. https://doi.org/10.1038/s41598-020-76726-7
34. Ivanova, N.; Andonova, V.; Jelev, I.; Dimova, G. Synthesis of silver nanoparticles with green tea-extracted reductants: a preliminary study for optimization of the preparation technique. *Scripta Scientifica Pharmaceutica* **2021**, *8(2)*, 17-26. http://dx.doi.org/10.14748/ssp.v8i2.8453
35. Repetto, G.; del Peso, A.; Zurita, J. L. Neutral red uptake assay for the estimation of cell viability/cytotoxicity. *Nature Protocols* 2008, *3(7)*, 1125–1131. https://doi.org/10.1038/nprot.2008.75
36. Robb, Christina. S.; Geldart, S. E.; Seelenbinder, J. A.; Brown, P. R. Analysis of Green Tea Constituents by HPLC-FTIR. *Journal of Liquid Chromatography & Related Technologies* **2002**, *25(5),* 787–801. https://doi.org/10.1081/jlc-120003036
37. Xia, J.; Wang, D.; Liang, P.; Zhang, D.; Du, X.; Ni, D.; Yu, Z. Vibrational (FT-IR, Raman) analysis of tea catechins based on both theoretical calculations and experiments. *Biophysical Chemistry* **2020**, *256*, 106282. https://doi.org/10.1016/j.bpc.2019.106282
38. Theivasanthi, T.; Alagar, M. Electrolytic Synthesis and Characterization of Silver Nanopowder. *Nano Biomedicine and Engineering* **2012**, *4(2)*. https://doi.org/10.5101/nbe.v4i2.p58-65
39. Janardhanan, R.; Karuppaiah, M.; Hebalkar, N.; Rao, T. N. Synthesis and surface chemistry of nano silver particles. *Polyhedron* **2009**, *28(12)*, 2522–2530. https://doi.org/10.1016/j.poly.2009.05.038
40. Jemal, K.; Sandeep, B. V.; Pola, S. Synthesis, Characterization, and Evaluation of the Antibacterial Activity of Allophylus serratus Leaf and Leaf Derived Callus Extracts Mediated Silver Nanoparticles. *Journal of Nanomaterials* **2017**, *2017*, 1–11. https://doi.org/10.1155/2017/4213275
41. Mehta, B. K.; Chhajlani, M.; Shrivastava, B. D. Green synthesis of silver nanoparticles and their characterization by XRD. *Journal of Physics: Conference Series* **2017**, *836*, 012050. https://doi.org/10.1088/1742-6596/836/1/012050
42. Priyadarshini, B.; Selvan, S.; Narayanan, K.; Fawzy, A. Characterization of Chlorhexidine-Loaded Calcium-Hydroxide Microparticles as a Potential Dental Pulp-Capping Material. *Bioengineering* **2017**, **4(4)**, 59. https://doi.org/10.3390/bioengineering4030059
43. Barot, T.; Rawtani, D.; Kulkarni, P. Development of Chlorhexidine Loaded Halloysite Nanotube Based Experimental Resin Composite with Enhanced Physico-Mechanical and Biological Properties for Dental Applications. *Journal of Composites Science* **2020**, *4(2)*, 81. https://doi.org/10.3390/jcs4020081
44. Raso, E. M. G.; Cortes, M. E.; Teixeira, K. I.; Franco, M. B.; Mohallem, N. D. S.; Sinisterra, R. D. A new controlled release system of chlorhexidine and chlorhexidine: βcd inclusion compounds based on porous

silica. *Journal of Inclusion Phenomena and Macrocyclic Chemistry* **2009**, *67(1–2)*, 159–168. https://doi.org/10.1007/s10847-009-9692-9

45. Gao, X.-Y.; Wang, S.-Y.; Li, J.; Zheng, Y.-X.; Zhang, R.-J.; Zhou, P.; Yang, Y.-M.; Chen, L.-Y. Study of structure and optical properties of silver oxide films by ellipsometry, XRD and XPS methods. *Thin Solid Films* **2004**, *455–456*, 438–442. https://doi.org/10.1016/j.tsf.2003.11.242
46. Jeung, D.-G.; Lee, M.; Paek, S.-M.; Oh, J.-M. Controlled Growth of Silver Oxide Nanoparticles on the Surface of Citrate Anion Intercalated Layered Double Hydroxide. *Nanomaterials* **2021**, *11(2)*, 455. https://doi.org/10.3390/nano11020455
47. Dhoondia, Z. H.; Chakraborty, H. Lactobacillus Mediated Synthesis of Silver Oxide Nanoparticles. *Nanomaterials and Nanotechnology* **2012**, *2*, 15. https://doi.org/10.5772/55741
48. Liu, J.; Lu, J.; Kan, J.; Wen, X.; Jin, C. Synthesis, characterization and in vitro anti-diabetic activity of catechin grafted inulin. *International Journal of Biological Macromolecules* **2014**, *64*, 76–83. https://doi.org/10.1016/j.ijbiomac.2013.11.028
49. Yin, I. X.; Zhang, J.; Zhao, I. S.; Mei, M. L.; Li, Q.; Chu, C. H. The Antibacterial Mechanism of Silver Nanoparticles and Its Application in Dentistry. *International Journal of Nanomedicine* **2020**, *15*, 2555–2562. https://doi.org/10.2147/ijn.s246764
50. Dakal, T. C.; Kumar, A.; Majumdar, R. S.; Yadav, V. Mechanistic Basis of Antimicrobial Actions of Silver Nanoparticles. *Frontiers in Microbiology* **2016**, *7*, 1831. https://doi.org/10.3389/fmicb.2016.01831